Journal of Power Sources 195 (2010) 8331–8335

Contents lists available at ScienceDirect

Journal of Power Sources

journal homepage: www.elsevier.com/locate/jpowsour

Short communication

Improved electrochemical performances of $9LiFePO_4 \cdot Li_3V_2(PO_4)/C$ composite prepared by a simple solid-state method

J.Y. Xiang, J.P. Tu*, L. Zhang, X.L. Wang, Y. Zhou, Y.Q. Qiao, Y. Lu

State Key Laboratory of Silicon Materials and Department of Materials Science and Engineering, Zhejiang University, Zheda Road, No. 38, Hangzhou 310027, Zhejiang, China

ARTICLE INFO

Article history:
Received 21 February 2010
Received in revised form 22 June 2010
Accepted 23 June 2010
Available online 30 June 2010

Keywords:
Lithium metal phosphate
Composite
Cathode
Lithium ion battery

ABSTRACT

$9LiFePO_4 \cdot Li_3V_2(PO_4)_3/C$ is synthesized via a carbon thermal reaction using petroleum coke as both reduction agent and carbon source. The as-prepared material is not a simple mixture of $LiFePO_4$ (LFP) and $Li_3V_2(PO_4)_3$ (LVP), but a composite possessing two phases: one is V-doped LFP and the other is Fe-doped LVP. The typical structure enhances the electrical conductivity of the composite and improves the electrochemical performances. The first discharge capacity of 9LFP·LVP/C in 18650 type cells is 168 mAh g^{-1} at 1 C (1 $C_{9LFP \cdot LVP/C}$ = 166 mA g^{-1}), and exhibits high reversible discharge capacity of 125 mAh g^{-1} at 10 C even after 150 cycles. At the temperature of −20 °C, the reversible capacity of 9LFP·LVP/C can maintain 75% of that at room temperature.

1. Introduction

Since Padhi et al. [1] firstly reported that lithium iron phosphate was a potential cathode for lithium ion batteries, many works had been devoted to preparing transition metal polyanion materials based on PO_4^{3-}, such as orthorhombic $LiMPO_4$ (M = Fe, Mn, Co) and monoclinic $Li_3M'_2(PO_4)_3$ (M′ = Fe, V) [2,3]. Among these materials, $LiFePO_4$ (LFP) and $Li_3V_2(PO_4)_3$ (LVP) attract the most attention for their high specific capacities (170 mAh g^{-1} and 194 mAh g^{-1}, respectively) as well as low cost. Although LFP is considered as the most promising high-rate cathode candidate [4], it should be treated with carbon coating [5], metal-rich phosphide nanonetworking [6], or super-valence ion doping [7–12] to facilitate the migration of electron and Li^+. For LVP, though Li^+ can transfer fast in its open three-dimensional framework, the high-rate property is somewhat disappointing for its poor electrical conductivity [13–15]. Moreover, the synthesis temperature of LVP is extremely high (higher than 850 °C) [16].

In order to simplify the synthesis process and improve the electrochemical properties of the electrode material as well, we firstly report a simple solid-state synthesis of *x*LFP·*y*LVP/C composites using micro-size petroleum coke as both reduction agent and carbon source. The microstructure and composition of the composites are discussed and the electrochemical performances at different rates and working temperatures are investigated.

2. Experimental

Stoichiometric Li_2CO_3, $NH_4H_2PO_4$, $FePO_4 \cdot 4H_2O$, NH_4VO_3 and micro-size petroleum coke were dispersed in alcohol, and then ball milled in a planetary mill for 15 h with agate ball and agate jar. The mass ratio of ball to powder was 10:1 and the rotation speed was 350 rpm. After alcohol was completely evaporated, the precursor was collected and sintered at 650 °C for 8 h in argon flow to obtain *x*LFP·*y*LVP/C composites.

The structure and composition of the samples were characterized by X-ray diffraction (XRD, Philips PC-APD with Cu Kα radiation), transmission electron microscopy (TEM, JEOL JEM-2010F) and energy dispersive spectrometer (EDS, GENENIS 4000), respectively. Electrical conductivity measurements were carried on a conductivity meter. The powders were uniaxially hot-pressed at 700 °C, 80 MPa for 1 h in vacuum.

The electrochemical performances were investigated in 18650 type cells assembled in an argon glove box. The cathode was prepared by coating the slurry consisted of 87 wt.% as-prepared particles, 8 wt.% graphite and 5 wt.% PVDF on aluminum foil. The mesocarbon microbead coating on copper foil was used as the anode. 1.0 M (0.9$LiBF_4$–0.1LiBOB) in PC–EC–EMC (1:1:3 in volume) was used as the electrolyte. The galvanostatic charge–discharge tests were conducted on LAND battery program-control test system at different discharge rates and different working temperatures in the voltage range of 2.5–4.3 V (vs. Li/Li^+). The capacity was calculated based on *x*LFP·*y*LVP/C. Cyclic voltammogram (CV) and electrochemical impedance spectroscopy (EIS) were performed on CHI660C electrochemical workstation. A three-electrode cell was used for EIS test, where

* Corresponding author. Tel.: +86 571 87952856; fax: +86 571 87952573.
E-mail address: tujp@zju.edu.cn (J.P. Tu).

0378-7753/$ – see front matter © 2010 Elsevier B.V. All rights reserved.
doi:10.1016/j.jpowsour.2010.06.070

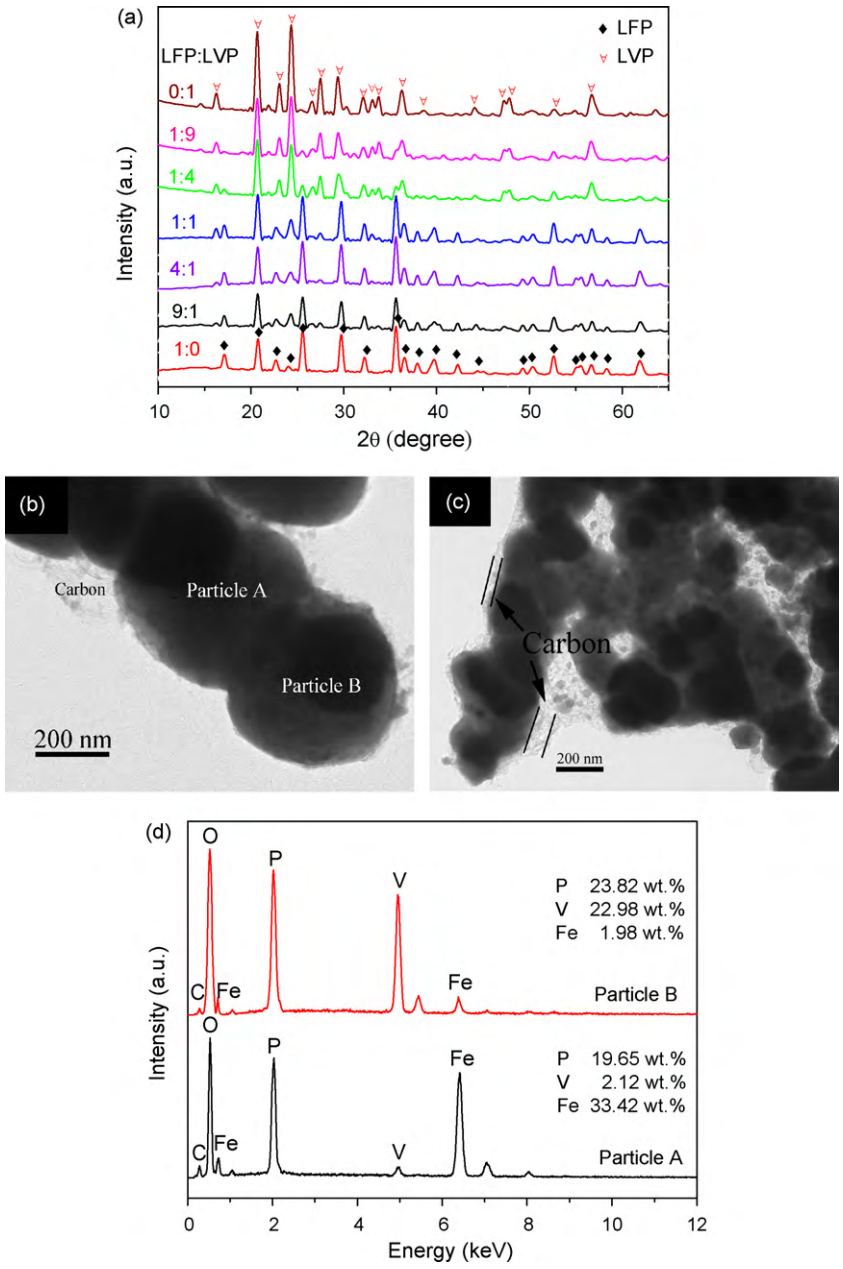

Fig. 1. (a) XRD patterns of xLiFePO$_4$·yLi$_3$V$_2$(PO$_4$)$_3$/C composites, (b) and (c) TEM images and (d) EDS spectrum of 9LiFePO$_4$·Li$_3$V$_2$(PO$_4$)$_3$/C.

lithium foils act as both the counter and reference electrodes.

3. Results and discussion

Fig. 1a shows the XRD patterns of the as-prepared xLFP·yLVP/C. When x:y = 1:0 and 0:1, all the diffraction peaks correspond well to orthorhombic LFP (space group *Pmnb* (62), JCPDS 40-1499) and monoclinic LVP (space group $P2_1/n$ (14), JCPDS 47-0107), respectively. When x:y = 9:1, 4:1, 1:1, 1:4 and 1:9, both the peaks of orthorhombic LFP and monoclinic LVP appear in the XRD patterns of the as-prepared materials. Besides, there is no evidence of diffraction peaks of carbon in all the products, which indicates the coated carbon is amorphous or the carbon quantity is too small to be detected. The solid-state reaction is described as follows:

$$4NH_4VO_3 + 3Li_2CO_3 + 6NH_4H_2PO_4 + 2C \rightarrow 2Li_3V_2(PO_4)_3 + 5CO_2 + 10NH_3 + 11H_2O \quad (1)$$

$$2FePO_4{\cdot}H_2O + Li_2CO_3 + C \rightarrow 2LiFePO_4 + CO_2 + 8H_2O + CO \quad (2)$$

The lattice constants of LFP/C, LVP/C and xLFP·yLVP/C (x:y = 9:1) are listed in Table 1. It is discovered that the cell sizes of LFP and LVP in the composite slightly change. For LFP, the one in the composite shrinks *a*-, *b*- and *c*-axis by 0.064%, 0.361% and 0.186% compared with the pristine one, respectively. For LVP, the one in composite shrinks *a*- and *c*-axis by 0.260% and 0.081%, and expands *b*-axis

Table 1
Unit cell parameters of LFP/C, LVP/C and 9LFP·LVP/C.

Material	Unit cell parameters			
	a (nm)	b (nm)	c (nm)	V (nm^3)
LFP/C	1.06257	0.63365	0.46854	0.31547
LVP/C	0.86859	1.20627	0.85638	0.89728
LFP in 9LFP·LVP	1.06189	0.63136	0.46767	0.31354
LVP in 9LFP·LVP	0.86633	1.21258	0.85569	0.89890

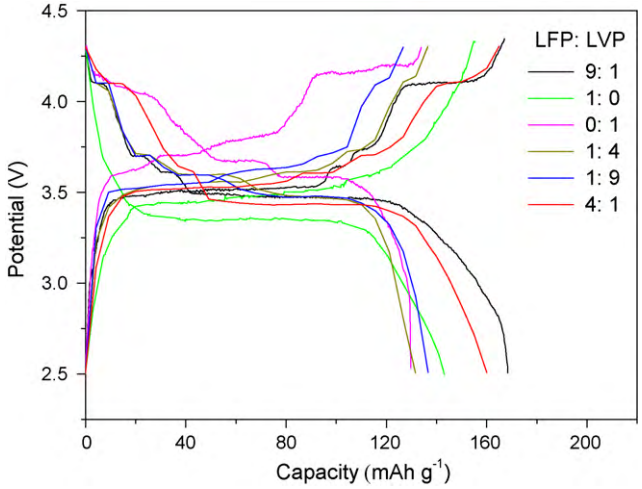

Fig. 2. The first charge/discharge curves of the xLiFePO$_4$·yLi$_3$V$_2$(PO$_4$)$_3$/C composites.

by 0.523% compared with the pristine one, respectively. The cell volume of LFP shrinks 0.612% while LVP expands 0.181% in the composite compared with those of pristine LFP and LVP. The slight changes in cell sizes indicate that doping occurs in the xLFP·yLVP/C composites ($x, y \neq 0$). It is even supposed that LFP in the composite is doped with V, and LVP in the composite is doped with Fe.

In order to further characterize the structure of xLFP·yLVP/C composites ($x, y \neq 0$), TEM images of 9LFP·LVP/C are presented in Fig. 1b and c. It can be seen that the particles are uniform with diameters of 300–500 nm. Amorphous carbon layer is coated well on the surface of the particles. The EDS spectrum of two adjacent particles in Fig. 1b is shown in Fig. 1d. Both the two particles contain Fe and V elements, but the molar rate of the elements is quite different. For particle A, the molar rate of Fe to P is nearly 1:1, which is close to that of LiFePO$_4$. And the content of V in particle A is relative low. For particle B, the molar rate of V to P is nearly 2:3 which is close to that of Li$_3$V$_2$(PO$_4$)$_3$. And the content of Fe in particle B is relative low. Obviously, the particles A and B are V-doped LFP and Fe-doped LVP, respectively. It is a good evidence for the assumption mentioned above that the as-prepared xLFP·yLVP/C composites ($x, y \neq 0$) possesses two phases: one is V-doped LFP and the other is Fe-doped LVP. In addition, the content of carbon in all the xLFP·yLVP/C composites are about 5.0 wt.% measured by elemental analysis.

Fig. 2 shows the initial charge–discharge curves of the xLFP·yLVP/C composites at 1 C (charge rate: 1 $C_{xLFP \cdot yLVP} = (170x + 132y)/(x + y)$ mA g^{-1}) from 2.5 V to 4.3 V. All the electrodes show similar charge–discharge behaviors. During the charging process, long plateaus appear around 3.5 V, corresponding to the phase transition from LiFePO$_4$ to FePO$_4$. The three subsequent plateaus around 3.6 V, 3.7 V, and 4.1 V can be indexed to the transformation of Li$_3$V$_2$(PO$_4$)$_3$ to Li$_x$V$_2$(PO$_4$)$_3$, where x = 2.5, 2, and 1, respectively [17]. It can be clearly seen that different contents of LFP and LVP phases in the composites result in different electrochemical performances. The 9LFP·LVP/C composite exhibits the highest discharge capacity (168 mAh g^{-1}) and initial coulombic efficiency (98%) among all the composites.

The cycling performances of 9LFP·LVP/C at different rates and working temperatures are shown in Fig. 3a and b. At rates of 1 C, 5 C, 10 C and 15 C, the first discharge capacity of 9LFP·LVP/C in 18650 type cells is 168 mAh g^{-1}, 143 mAh g^{-1}, 131 mAh g^{-1} and 102 mAh g^{-1}, respectively. And the discharge capacity is 163 mAh g^{-1} after 80 cycles at 1 C and 125 mAh g^{-1} after 150 cycles at 10 C, respectively. Furthermore, at the temperature of 65 °C, 0 °C and −20 °C, the reversible capacity of 9LFP·LVP/C is 166 mAh g^{-1},

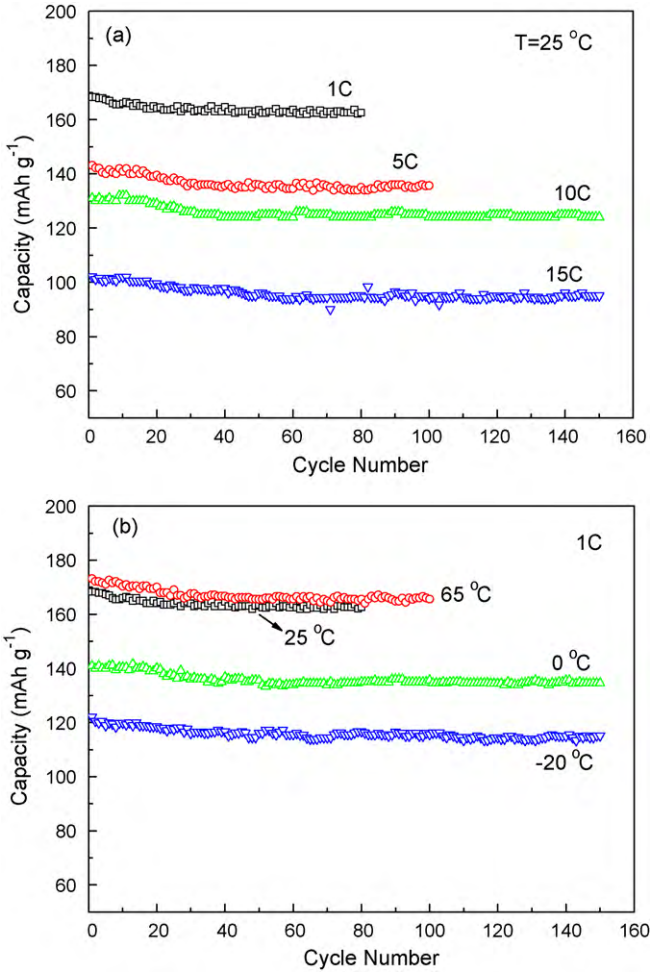

Fig. 3. Cycling performance of 9LiFePO$_4$·Li$_3$V$_2$(PO$_4$)$_3$/C: (a) at different discharge rates and (b) at different working temperatures.

134 mAh g^{-1} and 115 mAh g^{-1}, respectively. As can be seen, even at −20 °C, the capacity of 9LFP·LVP/C after 150 cycles still sustains 75% of that at room temperature. The improved electrochemical performances of 9LFP·LVP/C is greatly attributed to the enhanced electrical conductivity shown in Table 2. As can be seen, the electrical conductivity of 9LFP·LVP/C is improved to 2.50 × 10^{-2} S cm^{-1}, much higher than those of pristine LFP/C and LVP/C. It is also suggested that the excellent cycling performance at high rate and wide working temperature range is attributed to the interaction of V-doped LFP and Fe-doped LVP in the composite not only the V doping in LFP. As previous work reported, the electric conductivity of V-doped LFP is even lower than that of pure LFP, and V-doped LFP delivered specific capacity of about 100 mAh g^{-1} at 10 C [9], which is much lower than that of 9LFP·LVP/C. Moreover, the rate capability of 9LFP·LVP/C in the present work is also improved over previously reported LFP·LVP/C [18]. It is thus concluded that under the interaction of V-doped LFP and Fe-doped LVP, the electronic conductivity of 9LFP·LVP/C is greatly enhanced, and the rate capability and reversibility are significantly improved.

The physical characteristics of 18650 cell electrodes are shown in Table 3. It can be seen that the energy and power density of

Table 2
Electrical conductivities of LFP/C, LVP/C and 9LFP·LVP/C.

Material	LFP/C	LVP/C	9LFP·LVP/C
Electrical conductivity (S cm^{-1})	6.75 × 10^{-3}	2.88 × 10^{-3}	2.50 × 10^{-2}

Table 3
Physical characteristics of 18650 cell electrodes.

Characteristics	Electrodes		
	LFP/C	LVP/C	LFVP/C
Mass of the electrode material (g)	9.55	9.72	9.93
Mass of the active material (g)	8.33	8.46	8.64
Electrode area (cm^{-2}) (two side)	784	784	784
Surface density of the electrode material ($mg\,cm^{-2}$) (one side)	12.18	12.40	12.67
Capacity (mAh)	1200	1100	1400
Nominal voltage (V)	3.2	3.7	3.4
Mass of the cell (g)	34.3	34.6	35.1
Energy density ($Wh\,kg^{-1}$)	112	118	135
Power density at 15 C ($W\,kg^{-1}$)	680	626	805

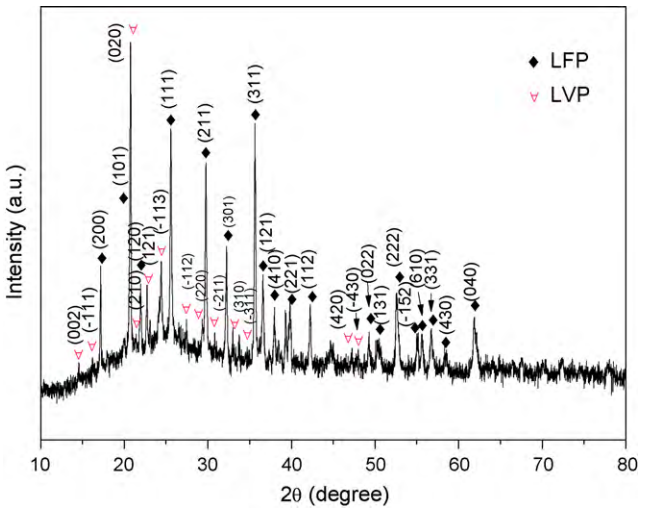

Fig. 4. XRD pattern of $9LiFePO_4{\cdot}Li_3V_2(PO_4)_3$/C after 20 cycles at 1 C.

9LFP·LVP/C are increased by 21% and 19% compared with the pristine LFP/C and LVP/C, respectively. The XRD pattern of 9LFP·LVP/C after 20 cycles at 1 C is shown in Fig. 4. The orthorhombic LFP and monoclinic LVP phases still sustain well in the composite, which also suggests the good cycling performance of 9LFP·LVP/C.

The initial cyclic voltammogram curves of LFP/C, LVP/C and 9LFP·LVP/C between 2.5 V and 4.3 V at a scan rate of 0.1 mV s^{-1} are presented in Fig. 5. The anodic and cathodic peaks correspond well with the charge–discharge plateaus shown in Fig. 2. The interval between anodic and cathodic peaks of 9LFP·LVP/C is smaller than

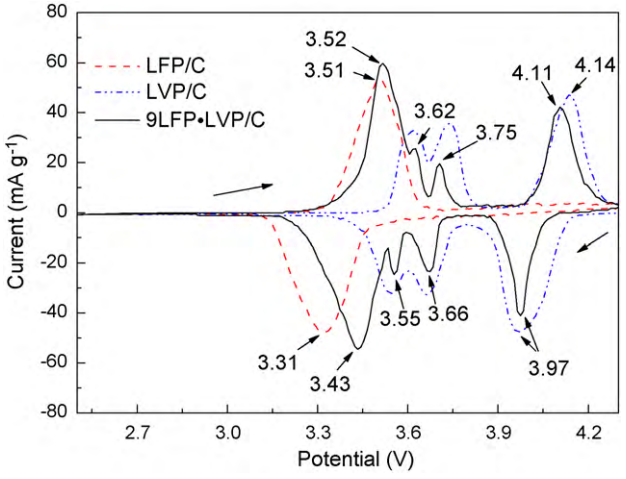

Fig. 5. Cyclic voltammogram curves at a scan rate of 0.1 mV s^{-1} from 2.5 V to 4.3 V.

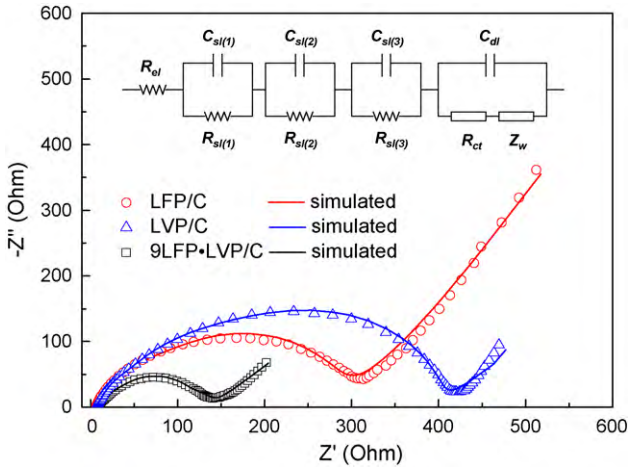

Fig. 6. Electrochemical impedance spectra measured at the discharge potential of 3.6 V in the 20th cycle.

those of pristine LFP/C and LVP/C, indicating the lower electrochemical polarization of 9LFP·LVP/C. Under the interaction of V-doped LFP and Fe-doped LVP, the electrical conductivity of 9LFP·LVP/C is improved and the electrode polarization is reduced, which results in the enhanced electrochemical properties.

EIS measurements were conducted in the frequency range of 100 kHz to 10 mHz at the discharge state (3.6 V) after 20 cycles. The Nyquist plots of the electrodes are shown in Fig. 6. Equivalent circuit and simulated curves are also provided. R_{el} represents the solution resistance; $R_{sl}(i)$ and $C_{sl}(i)$ (i = 1, 2 and 3) stand for the Li^+ migration resistance and capacity of surface layer, respectively; R_{ct} and C_{dl} designate the related charge-transfer resistance and double-layer capacitance, respectively; Z_W represents the diffusion-controlled Warburg impedance [19]. The simulated charge-transfer resistance R_{ct} of LFP/C, LVP/C and 9LFP·LVP/C are 60.1 Ω, 288.2 Ω and 16.1 Ω, respectively. The 9LFP·LVP/C composite exhibits the smallest R_{ct} value, which indicates the electrons and Li^+ can transfer more quickly on the interface of active materials and electrolyte. It is also an evidence for the improved electrical conductivity and enhanced reaction kinetics of the 9LFP·LVP/C composite, which possesses V-doped LFP and Fe-doped LVP at the same time.

4. Conclusions

$9LiFePO_4{\cdot}Li_3V_2(PO_4)_3$/C composite is synthesized by a simple solid-state method using petroleum coke as both reduction agent and carbon source. The composite shows enhanced electrochemical performance at high rate and wide working temperature range over pristine LFP/C and LVP/C. At 10 C, $9LiFePO_4{\cdot}Li_3V_2(PO_4)_3$/C exhibits reversible discharge capacity of 125 mAh g^{-1} even after 150 cycles. At temperature of −20 °C, the reversible capacity still remains 75% of that at room temperature. The improved electrochemical performances of $9LiFePO_4{\cdot}Li_3V_2(PO_4)_3$/C are attributed to the interaction of V-doped LFP and Fe-doped LVP, which increases the electronic conductivity and facilitate the insertion/extraction of lithium ions.

References

[1] A.K. Padhi, K.S. Najundaswamy, J.B. Goodenough, J. Electrochem. Soc. 144 (1997) 1188–1194.
[2] S.Y. Chung, J.T. Bloking, Y.M. Chiang, Nat. Mater. 1 (2002) 123–128.
[3] S.F. Yang, P.Y. Zavalij, M.S. Whittingham, Electrochem. Commun. 3 (2001) 505–508.
[4] B. Kang, G. Ceder, Nature 458 (2009) 190–193.
[5] M.M. Doeff, Y. Hu, F. Mclarnon, R. Kostecki, Electrochem. Solid-State Lett. 6 (2003) A207–209.
[6] P.S. Herle, B. Ellis, N. Coombs, L.F. Nazar, Nat. Mater. 3 (2004) 147–152.

[7] G. Wang, Y. Cheng, M.M. Yan, Z.Y. Jiang, J. Solid State Electrochem. 11 (2007) 457–462.
[8] J. Hong, C.S. Wang, U. Kasavajjula, J. Power Sources 162 (2006) 1289–1296.
[9] C.S. Sun, Z. Zhou, Z.G. Xu, D.G. Wang, J.P. Wei, X.K. Bian, J. Yan, J. Power Sources 193 (2009) 841–845.
[10] X.L. Li, F.Y. Kang, X.D. Bai, W.C. Shen, Electrochem. Commun. 9 (2007) 663–666.
[11] K.S. Park, J.T. Son, H.T. Chung, S.J. Kim, C.H. Lee, K.T. Kang, H.G. Kim, Solid State Commun. 129 (2004) 311–314.
[12] M. Wagemaker, B.L. Ellis, D. Lutzenkichen-Hecht, F.M. Mulder, L.F. Nazar, Chem. Mater. 20 (2008) 6313–6315.
[13] M.M. Ren, Z. Zhou, Y.Z. Li, X.P. Gao, J. Yan, J. Power Sources 162 (2006) 1357–1362.
[14] M. Sato, H. Ohkawa, K. Yoshida, M. Saito, K. Uematsu, K. Toda, Solid State Ionics 135 (2000) 137–142.
[15] L. Zhang, X.L. Wang, J.Y. Xiang, Y. Zhou, S.J. Shi, J.P. Tu, J. Power Sources 195 (2010) 5057–5061.
[16] M.Y. Saidi, J. Barker, H. Huang, J.L. Swoyer, G. Adamson, Electrochem. Solid-State Lett. 5 (2002) A149–A151.
[17] M.Y. Saidi, J. Barker, H. Huang, J.L. Swoyer, G. Adamson, J. Power Sources 119 (2003) 266–272.
[18] J.C. Zheng, X.H. Li, Z.X. Wang, S.S. Niu, D.R. Liu, L. Wu, L.J. Li, J.H. Li, H.J. Guo, J. Power Sources 195 (2010) 2935–12935.
[19] P. Suresh, A.K. Shukla, N. Munichandraiah, J. Appl. Electrochem. 32 (2002) 267–273.